第43卷 第1期 岩 石 矿 物 学 杂 志 Vol. 43, No. 1: 37~46
2024年1月 ACTA PETROLOGICA ET MINERALOGICA Jan., 2024

Doi: 10.20086/j.cnki.yskw.2024.0103

黑云母温度计能否用于估计花岗质侵入岩的结晶温度?

徐鸿雪,汪 洋

(中国地质大学(北京) 地球科学与资源学院, 北京 100083)

摘 要: 为了探讨黑云母温度计是否适用于估计花岗质侵入岩的结晶温度,汇编了国内外典型花岗质侵入体的岩石化学和矿物化学数据,利用Henry等(2005)的黑云母Ti饱和温度计、Li和Zhang(2022)的黑云母全组分温度计估算了岩浆温度,并与Shao等(2020)的锆饱和温度计估算结果进行了对比。结果表明,黑云母Ti饱和温度计估算的温度比锆饱和温度计和黑云母全组分温度计低50~200℃,因此认为黑云母Ti饱和温度计并不适用于估算花岗质侵入岩的结晶温度,而黑云母全组分温度计可以复现S型和I型花岗岩的锆饱和温度计结果。

关键词: 花岗质侵入体;结晶温度;黑云母Ti饱和温度计;黑云母温度计;锆饱和温度计

中图分类号: P588.12^{+}1 **文献标识码:** A **文章编号:** 1000-6524(2024)01-0037-10

Can biotite geothermometer be used to estimate the crystallization temperature of granitic intrusive rocks ?

XU Hong-xue and WANG Yang

(School of Earth Sciences and Resources, China University of Geosciences (Beijing), Beijing 100083, China)

Abstract: In order to investigate whether the biotite thermometer is suitable for estimating crystallization temperature of granite intrusive rocks, a compilation of the petrochemistry and mineral chemistry data of typical granitic intrusive rocks at domestic and abroad was made. The magma temperature was estimated using Henry *et al.* (2005) biotite Ti saturation geothermometer and the Li and Zhang (2022) version of the biotite geothermometer, and the results were compared with those estimated by the zircon saturation geothermometer in Shao *et al.* (2020). The results show that the temperatures estimated by the biotite Ti saturation geothermometer are 50~200℃ lower than those estimated by the zircon saturation geothermometer and the 2022 version of the biotite geothermometer. The biotite Ti saturation thermometer is not suitable for estimating the crystallization temperature of granitic intrusive rocks, while the Li and Zhang (2022) version of the biotite thermometer can reproduce the results of the zircon saturation thermometer for S-type and I-type granites.

Key words: granitic intrusive rock; crystallization temperature; biotite Ti saturation geothermometer; biotite geothermometer; zirconium saturation geothermometer

Fund support: Project of China Geological Survey (D1912)

收稿日期: 2023-07-05; **接受日期:** 2023-11-09; **编辑:** 郝艳丽

基金项目: 中国地质调查局地质调查项目(D1912)

作者简介: 徐鸿雪(1999-), 女, 硕士研究生, 地质工程专业, E-mail: xuhongxue163@163.com; 通讯作者: 汪 洋(1969-), 男, 主要从事岩石学和地热学研究, E-mail: allen_thalassa@sina.com。

岩浆结晶温度是理解火成岩成因的重要物理参量,环境和岩浆自身温度的变化控制了源岩部分熔融的发生、母岩浆的分离结晶以及岩体侵位后的固结过程(Miller *et al.*, 2003; Anderson *et al.*, 2008; Putirka, 2008)。对于特定成分的岩浆,温度和压力的变化对其平衡矿物组合起着决定性的作用,进而控制了岩浆岩的主量元素组成,影响岩浆岩的微量元素含量(Janousek and Moyen, 2020)。对于广义的花岗质岩浆而言,其温度范围大致在650~950℃之间。对于花岗质侵入岩,估算其结晶温度的主要方法包括两大类地质温度计。一类是(微量)元素饱和温度计,主要有锆饱和温度计、磷饱和温度计、钛饱和温度计、轻稀土元素饱和温度计等(Watson and Harrison, 1983; Harrison and Watson, 1984; Bea *et al.*, 1992; Pichavant *et al.*, 1992; Montel, 1993; Wolf and London, 1994; Jung and Pfänder, 2007; Stepanov *et al.*, 2012; Boehnke *et al.*, 2013; Shao *et al.*, 2019, 2020),近年来发展起来的锆石Ti温度计等(Janousek and Moyen, 2020)也属于此类。另一类是矿物温度计,包括钛铁矿-磁铁矿温度计、二长石温度计、辉石温度计、角闪石温度计、黑云母温度计等(Fuhrman and Lindsley, 1988; Benisek *et al.*, 2004; Henry *et al.*, 2005; Ghiorso and Evans, 2008; Putirka, 2008, 2016; Ridolfi *et al.*, 2010; Wang *et al.*, 2021b; Li and Zhang, 2022)。由于黑云母在花岗质岩浆岩中广泛存在,所以黑云母Ti温度计(Henry *et al.*, 2005)被不少学者用于估算花岗质侵入岩的结晶温度(Cesare *et al.*, 2008; Bayati *et al.*, 2017; Moshefi *et al.*, 2018; Azadbakht *et al.*, 2020; Azer *et al.*, 2020; Baidya *et al.*, 2021; Zhao *et al.*, 2023;王栋等, 2023; 邹兴志等, 2023)。然而,Henry等(2005)的黑云母Ti温度计是基于泥质变质岩的研究确立的,能否应用于花岗岩尚存疑义,该温度计估算的花岗质岩浆的温度是否准确亦缺乏实质性检验,为此本文应用经验性的方法检验了黑云母温度计估算花岗质侵入岩形成温度的可靠性。

1 估算花岗质侵入岩成岩温度的常用方法概述

锆元素在天然硅酸盐熔体中以微量元素的形式存在,其物理化学行为受稀溶液定律(Henry定律)制约。Watson和Harrison(1983)基于实验岩石学研究证明,锆在熔体中的饱和度主要取决于熔体的成分和温度。相较于其他元素饱和温度计,锆饱和温度计的优势在于:长英质岩浆体系中锆石-熔体之间Zr分配系数的温度敏感程度高,而且锆石是花岗质岩浆的早期结晶相,化学稳定性高,结晶后不易被改造,因此研究者对岩浆体系的Zr饱和体系进行了大量实验标定,积累了丰富的实验数据(Dietrich, 1968; Watson, 1979; Dickinson and Hess, 1982; Harrison and Watson, 1983; Watson and Harrison, 1983; Ellison and Hess, 1986; Keppler, 1993; Baker *et al.*, 2002; Hanchar and Watson, 2003; Boehnke *et al.*, 2013; Zhang and Xu, 2016; Gervasoni *et al.*, 2016; Shao *et al.*, 2019, 2020)。同时,锆石是花岗质岩浆中普遍存在的副矿物相,可以在中性-酸性成分的硅饱和熔体中结晶出来。对于含有残留锆石的花岗质侵入岩,锆饱和温度反映其岩浆温度的上限值;对于不含残留锆石的花岗质侵入岩(如A型花岗岩),锆饱和温度可以代表其岩浆温度的下限值。所以,锆饱和温度计是目前用于估算花岗质侵入岩成岩温度的最常用方法,得到了广泛应用(Miller *et al.*, 2003; Collins *et al.*, 2016, 2020)。

相对于锆饱和温度计,其他的地质温度计在花岗岩成岩温度估算方面存在一些局限。对磷、钛饱和温度计的实验标定研究较少(Harrison and Watson, 1984; Pichavant *et al.*, 1992; Montel, 1993),应用实例也比较少。轻稀土元素饱和温度计主要适用于含独居石的S型花岗岩类的温度估计(Montel, 1993; Stepanov *et al.*, 2012),对于不含独居石的I型和A型花岗岩,不能采用轻稀土元素饱和温度计估算其成岩温度。由于不少花岗岩不含辉石、角闪石,加之辉石温度计的精度不高(Wieser *et al.*, 2023),辉石、角闪石温度计在对花岗质岩浆岩中的应用实例有限(Anderson *et al.*, 2008)。例如,典型的S型花岗岩不含普通角闪石,无法采用涉及角闪石的地质温度计估算S型花岗岩的温度。同时,针对普通角闪石成分得到的温度计不适用于碱性角闪石,所以,常见的角闪石温度计无法用于含碱性角闪石的A型花岗岩。对于估算花岗质岩浆成岩温度而言,钛铁矿-磁铁矿温度计受固相线温度之下再平衡因素的影响(Fuhrman and Lindsley, 1988; Benisek *et al.*, 2004; Ghiorso and Evans, 2008),在岩浆固结之后Fe、Ti离子仍然在钛铁矿-磁铁矿之间发生扩散交换,导致计算的温度值明显低于岩浆的固相线温度。二长石温度计存在同样的缺陷。所以,对估计

花岗质侵入岩的成岩温度而言，钛铁矿-磁铁矿温度计和二长石温度计应用得比较少。

目前，锆饱和温度计已发表多个版本，主要有 Watson 和 Harrison(1983)(简称 WH83)、Boehnke 等(2013)(简称 B13)、Gervasoni 等(2016)(简称 G16)、Shao 等(2020)(简称 S20)等。S20 在先前模型基础上改进使其适用范围扩展到所有过铝质到过碱质成分的镁铁质到长英质熔体。Shao 等(2020)的研究表明，在常见的岩浆温度范围内，不管是过铝质还是过碱质熔体，S20 模型的估算结果与 WH83 模型的偏差在±5%不确定性范围内，而 B13、G16 模型对相同成分熔体的温度估计值较 WH83、S20 模型系统偏低(图 1)。

综合上述，本文采用 Shao 等(2020)锆饱和温度计模型作为计算花岗质侵入岩成岩温度的参照值，以此评估黑云母温度计对花岗质侵入岩的适用性。

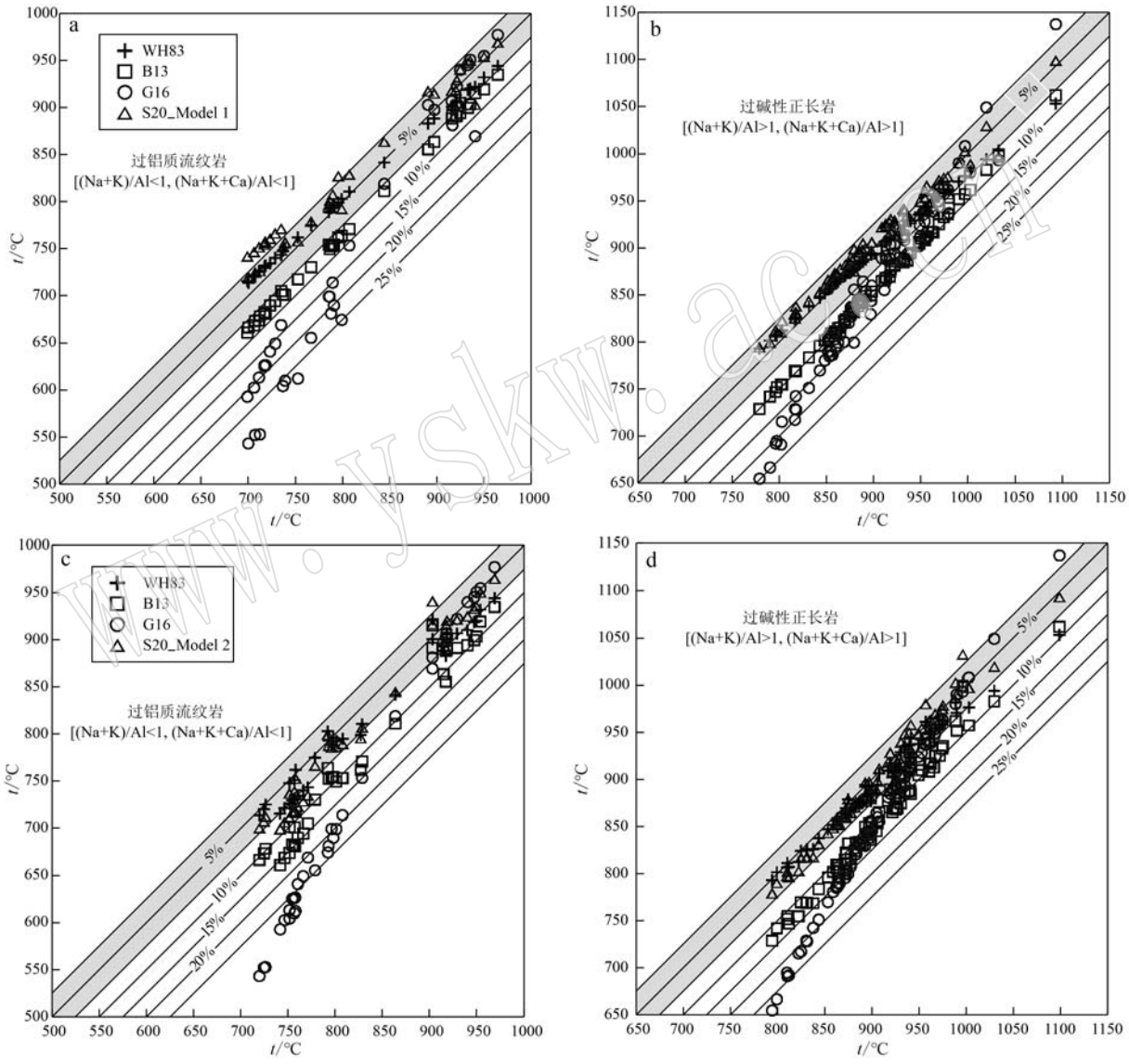

图 1　锆饱和温度计(S20)与其他版本锆饱和温度计(WH83、B13、G16)的估算结果对比[数据引自 Shao 等(2020)]

Fig. 1　The results of zirconium saturation thermometer (S20) compared with those of other versions of zirconium saturation thermometer (WH83, B13, G16) (data from Shao *et al.*, 2020)

a—S20 模型 1 与版本 WH83、B13、G16 对过铝质流纹岩计算结果对比；b—S20 模型 1 与版本 WH83、B13、G16 对过碱性正长岩计算结果对比；c—S20 模型 2 与版本 WH83、B13、G16 对过铝质流纹岩计算结果对比；d—S20 模型 2 与版本 WH83、B13、G16 对过碱性正长岩计算结果对比

a—comparison of S20 model 1 with other versions (WH83, B13, G16) on the calculation results of peraluminous rhyolite; b—comparison of S20 model 1 with other versions (WH83, B13, G16) on the calculation results of peralkaline syenite; c—comparison of S20 model 2 with other versions (WH83, B13, G16) on the calculation results of peraluminous rhyolite; d—comparison of S20 model 2 with other versions (WH83, B13, G16) on the calculation results of peralkaline syenite

本文的目的并非全面评估涉及花岗岩的地质温度计，对其他地质温度计的适用性等问题有待另文详述。

2 黑云母温度计的经验性检验

2.1 黑云母温度计概述

黑云母(包括狭义的黑云母和金云母)是地壳和地幔中广泛存在的一种含挥发分硅酸盐矿物，是大多数岩浆岩中的主要镁铁质造岩矿物之一，可在较大压力和温度范围内保持稳定。由于黑云母晶体结构比较复杂，能够大量地赋存多种阳离子和阴离子，其化学成分可以指示其形成的温度、氧逸度、水活度等重要参数，被广泛用于反演相关的岩浆性质和岩浆过程(Saha *et al.*, 2021; Samadi *et al.*, 2021; Gion *et al.*, 2022; Li and Zhang, 2022)。

Henry 等(2005)根据过铝质变泥质岩体系黑云母 Ti 含量与其形成温度的相关性，提出：

$$t=\left[\ln(\mathrm{Ti})+2.3594+1.7283(X_{\mathrm{Mg}})^{3}/b\right]^{0.333} \quad (1)$$

式中，t 为温度(℃)，Ti 为按 22 个 O 原子为单位计算阳离子数后的原子数，$X_{\mathrm{Mg}}=\mathrm{Mg}^{2+}/(\mathrm{Mg}^{2+}+\mathrm{Fe}^{2+}+\mathrm{Fe}^{3+})$，$b=4.648\ 2\times10^{-9}$，公式适用范围为：$X_{\mathrm{Mg}}=0.275\sim1.000$，$\mathrm{Ti}^{4+}=0.04\sim0.60$ a. p. f. u.，$t=480\sim800$℃。黑云母 Ti 温度计的精度估计，在较低温度范围内为±24℃，在较高温度下提高到±12℃。该温度计被国内外许多学者应用于估计花岗质侵入体的结晶温度(李胜荣等, 2006; Cesare *et al.*, 2008; 郭耀宇等, 2015; Moshefi *et al.*, 2018; Azadbakht *et al.*, 2020; 王栋等, 2023; 解世雄等, 2023; Zhao *et al.*, 2023)。

Henry 等(2005)指出，黑云母 Ti 温度计适用条件是含石墨、至少一种(黑云母之外的)过铝矿物、含钛铁矿或金红石的过铝质变质泥岩体系。虽然该温度计可能适用于过铝质成分的花岗岩，但对于其他成分的体系(例如准铝质花岗岩)而言，其实际误差可能十分显著(Henry, 私人通讯，见 Azadbakht *et al.*, 2020, p. 13)。

由于黑云母的化学结构复杂性，基于恒定的元素分配系数 K_{d} 估计黑云母和熔体平衡温度的传统方法不可行，例如，平衡体系中黑云母和熔体之间的 Mg/Fe 分配系数在黑云母-熔体体系中通常不是一个恒定值。因此，Li 和 Zhang (2022)在高温高压实验大数据的基础上，运用机器学习方法对岩浆成因黑云母矿物主要氧化物组分进行了回归训练，得到黑云母全组分与其形成温度、压力值的统计预测模型，提出了基于黑云母全组分的岩浆体系温压计(https://lixiaoyan.shinyapps.io/Biotite_thermobarometer/)。该文作者认为，黑云母全组分温度计可以较好地复现已有的实验标定温度，而 Henry 等(2005)黑云母 Ti 温度计则不能。

2.2 数据来源

本文汇编了来自全球不同区域的代表性花岗质侵入岩全岩和黑云母成分数据，根据原始文献描述，岩石和矿物样品新鲜，黑云母属于岩浆成因。根据岩相学和岩石地球化学特征，将这些样品分别归为S型、I型和A型花岗岩类(表1)。以Shao等

表 1 岩体名称及来源文献

Table 1 Names and reference of pluton

类型	地区	岩体/岩基	数据来源
S型	英国	Bodmin	Simons *et al.*, 2016
	英国	Carnmenellis	Simons *et al.*, 2016
	英国	Carn Marth	Simons *et al.*, 2016
	英国	Land's End	Simons *et al.*, 2016
	英国	Cligga	Simons *et al.*, 2016
	英国	Dartmoor	Simons *et al.*, 2016
	英国	St. Austell	Simons *et al.*, 2016
	意大利	Sattelspitze (Monte Sella)	Thöny *et al.*, 2009
	喜马拉雅山	Mount Qomolangma-Masang Kang	Visona *et al.*, 2012
	阿根廷	Tuani	Dahlquist *et al.*, 2005
	巴西	Nanuque	Ferreira *et al.*, 2019
	阿根廷	Mazan	Ferreira *et al.*, 2019
	阿根廷	Señor de la Peña	Ferreira *et al.*, 2019
	阿根廷	Capillitas	Ferreira *et al.*, 2019
	智利	Los Tilos	Ferreira *et al.*, 2019
	德国	Mitterteich	Siebel, 1995
	中国	峡江县金滩	Tao *et al.*, 2018
I型	瑞士	central Aar	Bucher and Seelig, 2018
	中国	阿尔泰造山带 Xibodu	Cui *et al.*, 2022
	加拿大	New Brunswick Lake George	Yang *et al.*, 2002
	巴西	Serra da Garganta	Nascimento *et al.*, 2018
	中国	秦岭丹凤蟒岭	杨阳等, 2022
	中国	薄竹山	Wang *et al.*, 2021a
	中国	秦岭沙河湾	刘春花等, 2013b
	中国	秦岭东江口、柞水	刘春花等, 2013a
	中国	铜山岭	Huang *et al.*, 2018
	韩国	Eopyeong 钾玄质侵入岩	Im *et al.*, 2021
A型	巴西	Campina do Veado rapakivi	Godoy *et al.*, 2021
	瑞士	Bristen	Bucher and Seelig, 2018
	中国	阿尔泰造山带 West Kouan	Cui *et al.*, 2022
	中国	陂头	Jiang *et al.*, 2022
	中国	黄梅尖	Zhang *et al.*, 2022
	尼日利亚	Ririwai 碱性杂岩体	Kinnaird *et al.*, 1985
	巴西	Mandira	Siachoque *et al.*, 2021
	巴西	Serra da Graciosa	Gualda and Vlach, 2007
	喀麦隆	Sabongari 碱性杂岩体	Njonfang *et al.*, 2013

(2020)的锆饱和温度计计算结果为参照值,同时采用 Henry 等(2005)黑云母 Ti 饱和温度计、Li 和 Zhang(2022)黑云母全组分温度计估计对应样品的黑云母结晶温度,将其结果与参照值相比较,判断计算的黑云母结晶温度能否代表岩浆的成岩温度。

2.3　结果与分析

(1) S 型花岗岩

图 2a 为黑云母 Ti 饱和温度计(Henry *et al.*, 2005)与锆饱和温度计(Shao *et al.*, 2020)估算的 S 型花岗岩成岩温度对比;图2b为黑云母全组分温度计(Li and Zhang, 2022)与锆饱和温度计估算的 S 型花岗岩成岩温度对比。结果显示,黑云母 Ti 饱和温度计估算结果较 S20 锆饱和温度计系统偏低 50 ~ 250℃,甚至低 500℃;黑云母全组分温度计的估算结果与 S20 锆饱和温度计之间的偏差大多在±50℃以内。因此,即便是对过铝质的 S 型花岗岩而言,黑云母 Ti 饱和温度计(Henry *et al.*, 2005)估算的温度值也是明显偏低的,因此该温度计并不适用于估算 S 型花岗岩的成岩温度。

(2) I 型花岗岩

从图 3 可知,大多数 I 型花岗岩样本的黑云母 Ti 饱和温度较 S20 锆饱和温度偏低 50~200℃,有相当数量的样品温度估算值低于 650℃(压力大于 100 MPa、饱和水条件下花岗岩的固相线温度)(图 3a)。黑云母全组分温度计的估算结果与 S20 锆饱和温度计之间的偏差绝大多数在±50℃以内(图 3b)。显然,黑云母 Ti 饱和温度计不适用于估算 I 型花岗岩的成岩温度。

(3) A 型花岗岩

图 4a 为黑云母 Ti 饱和温度计与 S20 锆饱和温度计估算的 A 型花岗岩成岩温度对比。从图中可以看出,黑云母Ti饱和温度计与S20锆饱和温度计估算

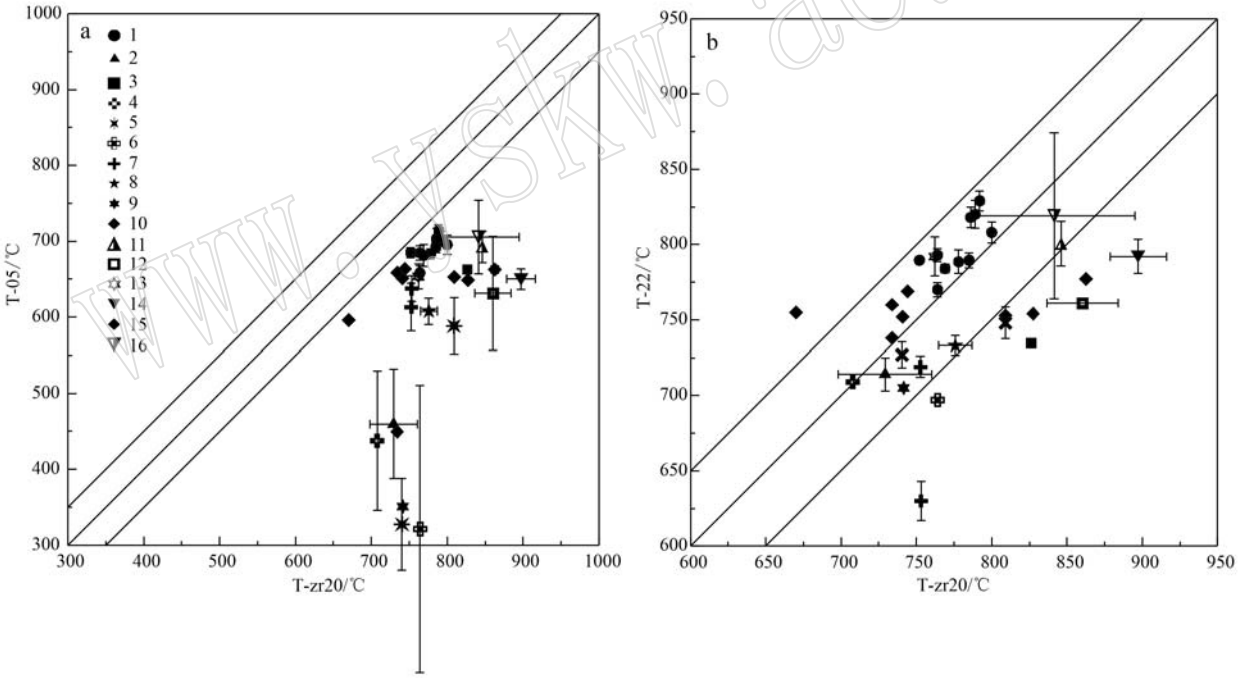

图 2　锆饱和温度计(Shao *et al.*, 2020)与黑云母 Ti 饱和温度计(Henry *et al.*, 2005)(a)、黑云母全组分温度计(Li and Zhang, 2022)(b)计算 S 型花岗岩温度结果对比图

Fig. 2　Comparison diagram of S-type granite temperature results calculated by zirconium saturation geothermometer (Shao *et al.*, 2020) and biotite Ti saturation geothermometer (Henry *et al.*, 2005) (a), biotite geothermometer (Li and Zhang, 2022) (b)

1—峡江县金滩(中国); 2—St. Austell (英国); 3—Dartmoor (英国); 4—Cligga (英国); 5—Land's End (英国); 6—Carn Marth (英国); 7—Carnmenellis (英国); 8—Bodmin (英国); 9—Sattelspitze (Monte Sella)(意大利); 10—Mount Qomolangma-Masang Kang(喜马拉雅山); 11—Señor de la Peña(阿根廷); 12—Mazún(阿根廷); 13—Capillitas(阿根廷); 14—Tuani(阿根廷); 15—Mitterteich(德国); 16—Nanuque(巴西)

1—Jintan, Xiajiang County (China); 2—St. Austell (UK); 3—Dartmoor (UK); 4—Cligga (UK); 5—Land's End (UK); 6—Carn Marth (UK); 7—Carnmenellis (UK); 8—Bodmin (UK); 9—Sattelspitze (Monte Sella) (Italy); 10—Mount Qomolangma-Masang Kang (Himalayas); 11—Señor de la Peña (Argentina); 12—Mazún (Argentina); 13—Capillitas (Argentina); 14—Tuani (Argentina); 15—Mitterteich (Germany); 16—Nanuque (Brazil)

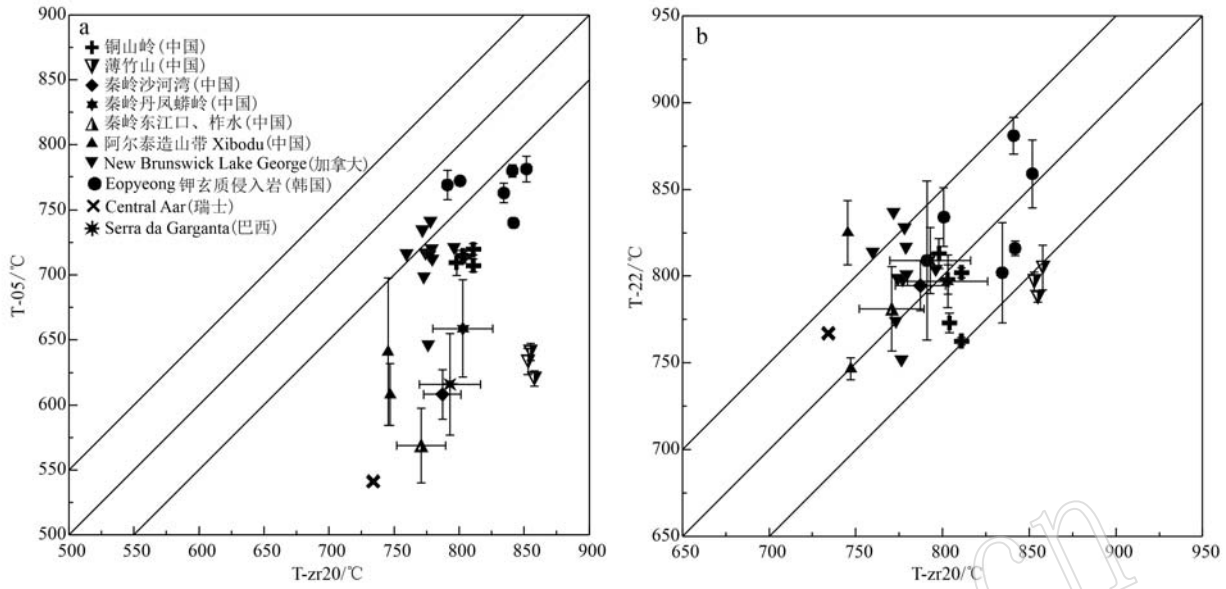

图 3 锆饱和温度计(Shao *et al.*, 2020)与黑云母 Ti 饱和温度计(Henry *et al.*, 2005)(a)、黑云母全组分温度计(Li and Zhang, 2022)(b)计算 I 型花岗岩温度结果对比图

Fig. 3 Comparison diagram of I-type granite temperature results calculated by zirconium saturation geothermometer (Shao *et al.*, 2020) and biotite Ti saturation geothermometer (Henry *et al.*, 2005) (a), biotite geothermometer (Li and Zhang, 2022) (b)

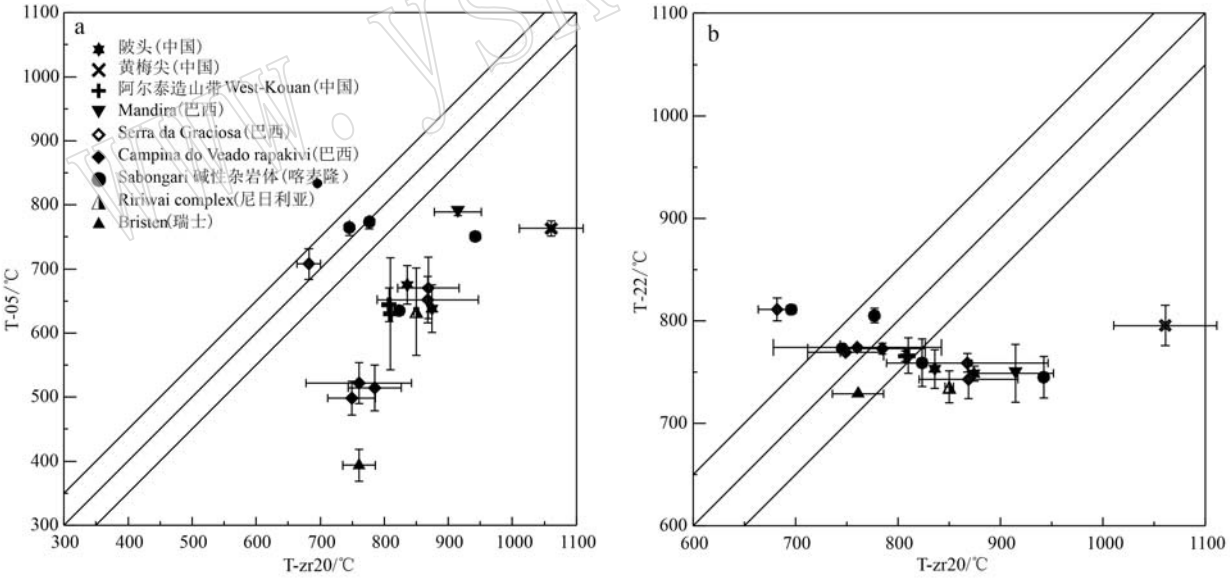

图 4 锆饱和温度计(Shao *et al.*, 2020)与黑云母 Ti 饱和温度计(Henry *et al.*, 2005)(图 a)、黑云母全组分温度计(Li and Zhang, 2022)(图 b)计算 A 型花岗岩温度结果对比图

Fig. 4 Comparison diagram of A-type granite temperature results calculated by zirconium saturation geothermometer (Shao *et al.*, 2020) and biotite Ti saturation geothermometer (Henry *et al.*, 2005) (a), biotite geotermometer (Li and Zhang, 2022) (b)

值之间具粗略的线性相关性,但黑云母 Ti 饱和温度明显低于锆饱和温度(约 100~300℃)。

黑云母全组分温度计与 S20 锆饱和温度计估算的 A 型花岗岩成岩温度之间则不存在明显的相关性(图 4b)。锆饱和温度计估算的 A 型花岗岩成岩温度在 670~1 100℃之间变化,黑云母全组分温度计得到的温度值介于 725~ 800℃之间。

A 型花岗质岩浆碱质含量高、对 Zr 的溶解能力

强(Gervasoni *et al.*, 2016; Shao *et al.*, 2020),因此 A 型花岗岩往往显示高的锆饱和温度,在某些情况下(如无继承锆石)A 型花岗质岩浆中 Zr 没有饱和,故而锆饱和温度计估算的成岩温度值偏低。对于准铝质和部分过碱性 A 型花岗岩,黑云母可视为近固相线矿物,其结晶温度低于液相线温度、高于固相线温度(Scaillet *et al.*, 2016)。所以黑云母全组分温度计给出的是 A 型花岗岩中黑云母的结晶温度,约束了相应岩浆体系固相线温度的上限值。

3　结论

(1) 无论是 S 型、I 型抑或 A 型花岗岩类,Henry 等(2005)黑云母 Ti 饱和温度计得到的成岩温度估算值较锆饱和温度计和黑云母全组分温度计的估算结果系统偏低 50 ~ 200℃以上,这表明对于花岗岩体系而言,黑云母 Ti 饱和温度计的估算结果地质意义不明确。因此 Henry 等(2005)黑云母 Ti 饱和温度计不适用于估算花岗质侵入岩的结晶温度。

(2) Li 和 Zhang(2022)发表的黑云母全组分温度计可以较好地复现 S 型和 I 型花岗质类的锆饱和温度计估算结果。碱质含量高的 A 型花岗质岩浆对 Zr 的溶解能力很强,导致 A 型花岗岩具有变化幅度较大的高 Zr 含量,其 Zr 饱和温度变化范围较大。对于 A 型花岗岩类,黑云母全组分温度计得到的温度值是黑云母在富碱质的花岗质岩浆体系中的结晶温度,在大多数情况下介于富碱质花岗质岩浆体系的液相线温度与固相线温度之间。

(3) Li 和 Zhang(2022)黑云母全组分温压计可作为一种独立于锆饱和温度计的方法用于估算 S 型和 I 型花岗质侵入岩的成岩温度,也可以用于约束 A 型花岗岩的固相线温度。

References

Anderson J L, Barth A P, Wooden J L, *et al*. 2008. Thermometers and thermobarometers in granitic systems[J]. Reviews in Mineralogy and Geochemistry, 69: 121~142.

Azadbakht Z, Lentz D R, McFarlane C R M, *et al*. 2020. Using magmatic biotite chemistry to differentiate barren and mineralized Silurian-Devonian granitoids of New Brunswick, Canada[J]. Contributions to Mineralogy and Petrology, 175: 69.

Azer M K, Surour A A, Madani A A, *et al*. 2020. Mineralogical and geochemical constraints on the postcollisional mafic magmatism in the Arabian-Nubian Shield: An example from the El-Bakriya Area, central Eastern Desert, Egypt[J]. The Journal of Geology, 130(3): 209~230.

Baidya A S, Pal D C and Upadhyay D. 2021. Biotite chemistry and mineral association as an indicator of redox conditions in the iron oxide Cu-Au (IOCG) system: Constraints from the Khetri Copper Belt. western India[J]. Ore Geology Reviews, 139(5): 104544.

Baker D R, Conte A, Freda C, *et al*. 2002. The effect of halogens on Zr diffusion and zircon dissolution in hydrous metaluminous granitic melts[J]. Contributions to Mineralogy and Petrology, 142: 666~678.

Bayati M, Esmaeily D, Maghdour-Mashhour R, *et al*. 2017. Geochemistry and petrogenesis of Kolah-Ghazi granitoids of Iran: Insights into the Jurassic Sanandaj-Sirjan magmatic arc[J]. Geochemistry, 77(2): 281~302.

Bea F, Fershtater G B and Corretgé L G. 1992. The geochemistry of phosphorus in granite rocks and the effects of aluminium[J]. Lithos, 29: 43~56.

Benisek A, Kroll H and Cemič L. 2004. New developments in two-feldspar thermometry[J]. American Mineralogist, 89(10): 1 496~1 504.

Boehnke P, Watson E B, Trail D, *et al*. 2013. Zircon saturation re-revisited[J]. Chemical Geology, 351: 324~334.

Bucher K and Seelig U. 2018. Bristen granite: A highly differentiated, fluorite-bearing A-type granite from the Aar massif, Central Alps, Switzerland[J]. Swiss Journal of Geosciences, 111: 317~340.

Cesare B, Satish-Kumar M, Cruciani G, *et al*. 2008. Mineral chemistry of Ti-rich biotite from pegmatite and metapelitic granulites of the Kerala Khondalite Belt (southeast India): Petrology and further insight into titanium substitutions[J]. American Mineralogist, 93: 327~338.

Collins W J, Huang H Q and Jiang X Y. 2016. Water-fluxed crustal melting produces Cordilleran batholiths[J]. Geology, 44(2): 143~146.

Collins W J, Murphy J B and Johnson T E *et al*. 2020. Critical role of water in the formation of continental crust[J]. Nature Geoscience, 13(5): 1~8.

Cui X, Sun M and Zhao G. 2022. Syn-orogenic A-type granites and post-collisional I-type granites in the southern Chinese Altai: Petrogenesis and implications for granite classification[J]. Gondwana Research, 111: 20~34.

Dahlquist J A, Rapela C W and Baldo E G. 2005. Petrogenesis of cordi-

erite-bearing S-type granitoids in Sierra de Chepes, Famatinian orogen, Argentina[J]. Journal of South American Earth Sciences, 20: 231~251.

Dickinson J E and Hess P C. 1982. Zircon saturation in lunar basalts and granites[J]. Earth and Planetary Science Letters, 57(2): 336~344.

Dietrich R V. 1968. Behavior of zirconium in certain artificial magmas under diverse P-T conditions[J]. Lithos, 1(1): 20~29.

Ellison A J and Hess P C. 1986. Solution behavior of +4 cations in high silica melts: Petrologic and geochemical implications[J]. Contributions to Mineralogy and Petrology, 94: 343~351.

Ferreira V P, Sial A N, Toselli A J, *et al*. 2019. Cordierite-bearing granitic rocks in South America: Contrasting sources and conditions of formation[J]. Journal of South American Earth Sciences, 92: 417~434.

Fuhrman M L and Lindsley D H. 1988. Ternary-feldspar modeling and thermometry[J]. American Mineralogist, 73 (3~4): 201~215.

Gervasoni F, Klemme S, Rocha Jr E R V, *et al*. 2016. Zircon saturation in silicate melts: a new and improved model for aluminous and alkaline melts[J]. Contributions to Mineralogy and Petrology, 171: 21.

Ghiorso M S and Evans B W. 2008. Thermodynamics of rhombohedral oxide solid solutions and a revision of the Fe-Ti two-oxide geothermometer and oxygen-barometer[J]. American Journal of Science, 308 (9): 957~1 039.

Gion A M, Piccoli P M and Candela P A. 2022. Characterization of biotite and amphibole compositions in granites[J]. Contributions to Mineralogy and Petrology, 177: 43.

Godoy A M, Vieira O A R P, de Godoy D F, *et al*. 2021. Geology, geochemistry and mineral chemistry of Campina do Veado and Santa Blandina Rapakivi granite stocks. Southwest of São Paulo State[J]. Revista Geociências, 40: 307~338.

Gualda G A R and Vlach S R F. 2007. The Serra da Graciosa A-type Granites and Syenites, southern Brazil Part 2: Petrographic and mineralogical evolution of the alkaline and aluminous associations[J]. Lithos, 93: 310~327.

Guo Yaoyu, He Wenyan, Li Zaichun, *et al*. 2015. Petrogenesis of Ge'erkuohe porphyry granitoid, western Qinling: Constraints from mineral chemical characteristics of biotites[J]. Acta Petrologica Sinica, 31(11): 3 380~3 390 (in Chinese with English abstract).

Hanchar J M and Watson E B. 2003. Zircon Saturation Thermometry[J]. Reviews in Mineralogy and Geochemistry, 53: 89~112.

Harrison T M and Watson E B. 1983. Kinetics of zircon dissolution and zirconium diffusion in granitic melts of variable water content[J]. Contributions to Mineralogy and Petrology, 84: 66~72.

Harrison T M and Watson E B. 1984. The behavior of apatite during crustal anatexis: Equilibrium and kinetic considerations[J]. Geochimica et Cosmochimica Acta, 48: 1 467~1 477.

Henry D J, Guidotti C V and Thomson J A. 2005. The Ti-saturation surface for low-to-medium pressure metapelitic biotites: Implications for geothermometry and Ti-substitution mechanisms[J]. American Mineralogist, 90(2~3): 316~328.

Huang X D, Lu J J, Sizaret S, *et al*. 2018. Reworked restite enclave: Petrographic and mineralogical constraints from the Tongshanling intrusion, Nanling Range, South China[J]. Journal of Asian Earth Sciences, 166: 1~18.

Im S, Park J W, Kim J, *et al*. 2021. Petrogenesis of coeval shoshonitic and high-K calc-alkaline igneous suites in the Eopyeong granitoids, Taebaeksan Basin, South Korea: Lithospheric thinning-related Early Cretaceous magmatism in the Korean Peninsula[J]. Lithos, 392~393: 106127.

Janousek V and Moyen J F. 2020. Whole-rock geochemical modelling of granite genesis-the current state of play[C]//Janousek V, Bonin B, Collins W J, *et al*. Post-Archean Granitic Rocks: Petrogenetic Processes and Tectonic Environments. Geological Society, London, Special Publications, 491: 267~291.

Jiang Y H, Liu Y C, Han B N, *et al*. 2022. Contrasting origins of A-type granites in the Late Triassic-Early Jurassic Pitou complex, southern Jiangxi province: Implications for Mesozoic tectonic evolution in South China[J]. Lithos, 426~427: 106794.

Jung S, Pfänder J A. 2007. Source composition and melting temperatures of orogenic granitoids: Constraints from CaO/Na_2O, Al_2O_3/TiO_2 and accessory mineral saturation thermometry[J]. European Journal of Mineralogy, 19(6): 859~870.

Keppler H. 1993. Influence of fluorine on the enrichment of high field strength trace elements in granitic rocks[J]. Contributions to Mineralogy and Petrology, 114: 479~488.

Kinnaird J A, Bowden P, Ixer R A, *et al*. 1985. Mineralogy, geochemistry and mineralization of the Ririwai complex, northern Nigeria[J]. Journal of African Earth Sciences, 3(1~2): 185~222.

Li Shengrong, Sun Li and Zhang Huafeng. 2006. Magma mixing genesis of the Qushui collisional granitoids, Tibet, China: Evidences from genetic mineralogy[J]. Acta Petrologica Sinica, 22(4): 884~894 (in Chinese with English abstract).

Li X and Zhang C. 2022. Machine learning thermobarometry for biotite-bearing magmas[J]. Journal of Geophysical Research: Solid Earth, 127(9): e2022JB024137.

Liu Chunhua, Wu Cailai, Lei Min, *et al*. 2013a. Mineral composition and temperature-pressure conditions of Dongjiangkou and Zhashui granites in the Qinling Mountains[J]. Acta Petrologica et Mineralogica, 32(3): 341~354 (in Chinese with English abstract).

Liu Chunhua, Wu Cailai, Lei Min, *et al*. 2013b. Petrology and mineralogy of the I-type granites and ternperature-pressure conditions for magma for mation in the Shahewan mass of the Qinling[J]. Geology and Exploration, 49(4): 595~608 (in Chinese with English abstract).

Miller C F, McDowell S M and Mapes R W. 2003. Hot and cold granites? Implications of zircon saturation temperatures and preservation of inheritance[J]. Geology, 31(6): 529~532.

Montel J M. 1993. A model for monazite/melt equilibrium and application to the generation of granitic magmas[J]. Chemical Geology, 110: 127~146.

Moshefi P, Hosseinzadeh M R, Moayyed M, *et al*. 2018. Comparative study of mineral chemistry of four biotite types as geochemical indicators of mineralized and barren intrusions in the Sungun Porphyry Cu-Mo deposit, northwestern Iran[J]. Ore Geology Reviews, 97: 1~20.

Nascimento M A L do, Medeiros V C de, Galindo A C, *et al*. 2018. Plúton Serra da Garganta como registro de magmatismo cálcio-alcalino no Domínio Rio Piranhas-Seridó. Nordeste da Província Borborema[J]. Pesquisas em Geociências, 45: e0620.

Njonfang E, Tchoneng G T, Cozzupoli D, *et al*. 2013. Petrogenesis of the Sabongari alkaline complex, Cameroon line (central Africa): Preliminary petrological and geochemical constraints[J]. Journal of African Earth Sciences, 83: 25~54.

Pichavant M, Montel J M and Richard L R. 1992. Apatite solubility in peraluminous liquids: Experimental data and extension of the Harrison-Watson model[J]. Geochimica et Cosmochimica Acta, 56: 3 855~3 861.

Putirka K D. 2008. Thermometers and barometers for volcanic systems [J]. Reviews in Mineralogy and Geochemistry, 69: 61~120.

Putirka K. 2016. Amphibole thermometers and barometers for igneous systems and some implications for eruption mechanisms of felsic magmas at arc volcanoes[J]. American Mineralogist, 101: 841~858.

Ridolfi F, Renzulli A and Puerini M. 2010. Stability and chemical equilibrium of amphibole in calc-alkaline magmas: An overview, new thermobarometric formulations and application to subduction-related volcanoes[J]. Contributions to Mineralogy and Petrology, 160: 45~66.

Saha R, Upadhyay D and Mishra B. 2021. Discriminating tectonic setting of igneous rocks using biotite major element chemistry-a machine learning approach[J]. Geochemistry, Geophysics, Geosystems, 22(11): e2021GC010053.

Samadi R, Torabi G, Kawabata H, *et al*. 2021. Biotite as a petrogenetic discriminator: Chemical insights from igneous, meta-igneous and meta-sedimentary rocks in Iran[J]. Lithos, 386~387: 106016.

Scaillet B, Holtz F and Pichavant M. 2016. Experimental constraints on the formation of silicic magmas[J]. Elements, 21: 109~114.

Shao T, Xia Y, Ding X, *et al*. 2019. Zircon saturation in terrestrial basaltic melts and its geological implications[J]. Solid Earth Sciences, 4: 27~42.

Shao T, Ying X, Ding X, *et al*. 2020. Zircon saturation model in silicate melts: A review and update[J]. Acta Geochimica, 39: 387~403.

Siachoque A, Santos C A and Vlach S R F. 2021. Amphiboles and phyllosilicates in the A-type Mandira Granite Massif, Graciosa Province, SE Brazil: Textures, composition and crystallisation conditions[J]. Mineralogical Magazine, 85: 784~807.

Siebel W. 1995. Constraints on Variscan granite emplacement in northeast Bavaria, Germany: Further clues from a petrogenetic study of the Mitterteich granite[J]. Geologische Rundschau, 84: 384~398.

Simons B, Shail R K and Andersen J C O. 2016. The petrogenesis of the Early Permian Variscan granites of the Cornubian Batholith: Lower plate post-collisional peraluminous magmatism in the Rhenohercynian Zone of SW England[J]. Lithos, 260: 76~94.

Stepanov A S, Hermann J, Rubatto D, *et al*. 2012. Experimental study of monazite/melt partitioning with implications for the REE, Th and U geochemistry of crustal rocks[J]. Chemical Geology, 300~301: 200~220.

Tao J, Li W, Wyman D A, *et al*. 2018. Petrogenesis of Triassic granite from the Jintan pluton in central Jiangxi Province, South China: Implication for uranium enrichment[J]. Lithos, 320~321: 62~74.

Thöny W F, Wyhlidal S, Tropper P, *et al*. 2009. Petrology of a cordierite-andalusite-bearing granite from the Sattelspitze (Monte Sella), Franzensfeste (South Tyrol, Italy)[J]. Mitteilungender Österreichischen Mineralogischen Gesellschaft, 155: 269~277.

Visona D, Carosi R, Montomoli C, *et al*. 2012. Miocene andalusite leucogranite in central-east Himalaya (Everest-Masang Kang area): Low-pressure melting during heating[J]. Lithos, 144~145: 194~208.

Wang Dong, Wang Tianqi and Li Hongyan. 2023. Petrogenesis of Early Cretaceous Laoshan A-type granites and the implications for the tectonic evolution of Jiaodong Peninsula[J]. Acta Petrologica Sinica, 39(2): 317~339 (in Chinese with English abstract).

Wang G C, Liu Z, Tan S C, *et al*. 2021a. Petrogenesis of biotite granite

with transitional I-A-type affinities: Implications for continental crust generation[J]. Lithos, 396~397: 106199.

Wang X, Hou T, Wang M, *et al*. 2021b. A new clinopyroxene thermobarometer for mafic to intermediate magmatic systems[J]. European Journal of Mineralogy, 33: 621~637.

Watson E B. 1979. Zircon saturation in felsic liquids: Experimental results and applications to trace element geochemistry[J]. Contributions to Mineralogy and Petrology, 70(4): 407~419.

Watson E B and Harrison T M. 1983. Zircon saturation revisited: Temperature and composition effects in a variety of crustal magma types[J]. Earth and Planetary Science Letters, 64(2): 295~304.

Wieser P E, Kent A J R, Till C B, *et al*. 2023. Barometers behaving badly I: Assessing the influence of analytical and experimental uncertainty on clinopyroxene thermobarometry calculations at crustal conditions[J]. Journal of Petrology, 64(2): egac126.

Wolf M B and London D. 1994. Apatite dissolution into peraluminous haplogranitic melts: An experimental study of solubilities and mechanisms[J]. Geochimica et Cosmochimica Acta, 58: 4 127~4 146.

Xie Shixiong, Chen Xilian, Huang Wenting, *et al*. 2023. Compositional characteristics of bitote in felsic igneous rocks and its geological implication in the Gejiu Sn-Cu polymetallic ore field, Yunnan Province[J]. Geochimica, 52(2): 212~221 (in Chinese with English abstract).

Yang X M, Hall D C, Chi G, *et al*. 2002. Petrology of the Lake George granodiorite stock, New Brunswick: Implications for crystallization conditions, volatile exsolution, and W-Mo-Au-Sb mineralization[J]. Ottawa: Natural Resources Canada Geological Survey of Canada, Current Research, E14: 1~12.

Yang Yang, Ke Changhui, Wang Xiaoxia, *et al*. 2022. Magmatic evolution and origin of Mangling granitic pluton in north Qinling, China: Evidence from mineralogy and Sr-Nd-Hf isotopes[J]. Journal of Earth Sciences and Environment, 44(4): 658~674 (in Chinese with English abstract).

Zhang L, Wang F, Zhou T, *et al*. 2022. The origin of uranium deposits related to the Huangmeijian A-type granite from the Lu-Zong volcanic basin, South China: Constraints from zircon U-Pb geochronology and mineral chemistry[J]. Ore Geology Reviews, 141: 104665.

Zhang Y and Xu Z. 2016. Zircon saturation and Zr diffusion in rhyolitic melts, and zircon growth geospeedometer[J]. American Mineralogist, 101(6): 1 252~1 267.

Zhao L, Li Y, Xiang H, *et al*. 2023. A Devonian shoshonitic appinite-granite suite in the North Qinling orogenic belt: Implications for partial melting of a water-fluxed lithospheric mantle in an extensional setting[J]. Journal of Petrology, 64: egad040.

Zou Xingzhi and Ren Tao. 2023. Mineralogical and geochemical characteristics of biotite from the Bozhushan granite in the Southeastern Yunnan and their implications for petrogenesis and mineralization[J]. Acta Mineralogica Sinica, 43(1): 83~92 (in Chinese with English abstract).

附中文参考文献

郭耀宇, 和文言, 李在春, 等. 2015. 西秦岭格尔括合花岗闪长斑岩岩石成因——黑云母矿物学特征约束[J]. 岩石学报, 31(11): 3 380~3 390.

李胜荣, 孙 丽, 张华锋. 2006. 西藏曲水碰撞花岗岩的混合成因: 来自成因矿物学证据[J]. 岩石学报, 22(4): 884~894.

刘春花, 吴才来, 雷 敏, 等. 2013a. 秦岭东江口和柞水花岗岩的矿物成分特征及其形成的温压条件[J]. 岩石矿物学杂志, 32(3): 341~354.

刘春花, 吴才来, 雷 敏, 等. 2013b. 秦岭沙河湾I型花岗岩岩石学、矿物学特征及岩浆形成的温压条件[J]. 地质与勘探, 49(4): 595~608.

王 栋, 王天齐, 李红艳. 2023. 胶东崂山早白垩世A型花岗岩成因及对区域构造演化的意义[J]. 岩石学报, 39(2): 317~339.

解世雄, 陈喜连, 黄文婷, 等. 2023. 云南个旧Sn-Cu多金属矿田中酸性岩黑云母特征及其成矿意义[J]. 地球化学, 52(2): 212~221.

杨 阳, 柯昌辉, 王晓霞, 等. 2022. 北秦岭蟒岭花岗岩体岩浆演化及源区——来自矿物学和Sr-Nd-Hf同位素证据[J]. 地球科学与环境学报, 44(4): 658~674.

邹兴志, 任 涛. 2023. 滇东南薄竹山雷达站花岗岩黑云母矿物化学特征与成岩成矿[J]. 矿物学报, 43(1): 83~92.